ATA memo 80 : June 2009

Antenna Gain, Pointing, Primary Beam and Bandpass Calibration

David MacMahon & Melvyn Wright

Radio Astronomy Laboratory, University of California, Berkeley, CA, 94720

ABSTRACT

In this memo we present a method for calibrating the antenna gain, pointing, and primary beam width of the ATA antennas from observations of compact sources in an interferometer mosaic pattern. The data are self-calibrated to determine the antenna voltage gains. Gaussian fits to antenna voltage patterns are used to analyze the ATA beam patterns at 1430, 1810, 2010, 3500 & 6500 MHz. For multichannel observations the antenna-based bandpass solutions are also measured. Several antennas have a large pointing squint. After omitting antennas with pointing squint the measured beamwidths are $\sim 5\%$ smaller than the current Gaussian model Since these observations are similar to mosaic projects we should get better mosaic imaging performance using the measured primary beam FWHM. The mean values for both axes are 149.7 +/- 4.0, 59.8 +/- 2.2, and 31.8 +/- 1.6 arcmin at 1430, 3500 and 6500 MHz respectively.

1. INTRODUCTION

The Allen Telescope Array is a widefield radio telescope which can make simultaneous observations in 4 tunable bands from 0.5 to 11 GHz (Welch etal. 2009). The telescope currently is comprised of 42 6m diameter antennas equipped with log periodic feeds and wideband amplifiers which deliver the entire 0.5 to 11 GHz band to a versatile digital back end.

The digital signal processing is configured with cross correlators and beamformers to observe simultaneously at multiple frequencies. The telescope can be reconfigured rapidly for multiple, simultaneous observing projects. For arrays with large numbers of antennas, the high data rates and need for real time processing of the data pose a challenge for quick and accurate calibration. High signal to noise in the calibration sources helps with quick and accurate calibration, but high SNR in the target sources also means that more accurate calibration is needed, or the observations will be limited by the calibration.

In this memo we present a method for calibrating the antenna gain, pointing, and primary beam width of the ATA antennas from observations of a compact sources in a hexagonal 7-pointing mosaic at the frequency and telescope settings being used for the observations. In this way, we can ensure that the data can be calibrated accurately in close to real time, as the data are aquired.

2. OBSERVATIONS AND DATA REDUCTION

Mosaic observations are obtained using a standard hexagonal 7-pointing mosaic of a strong compact source at the nominal pointing center and half power points for the 6m antennas. The data are self-calibrated to determine the antenna voltage gains. For quasars we used the MIRIAD task **mfcal** to determine the gain versus time and the bandpass. The voltage gains are determined for each pointing separately with respect to the flux density of the quasar.

The ruby script **gpfit.rb** was used to make Gaussian fits to the voltage gains to determine the pointing and primary beam width of each of the the ATA antennas. **gpfit.rb** makes tables of the peak value, pointing offset and voltage primary beamwidth from the Gaussian fits to the antenna gains for each antenna and solution interval. The ruby script **plotpbfits.rb** plots the fitted Gaussian pointing offset and primary beam FWHM, providing an easy to assimilate assessment of the antenna performance.

In this memo, we illustrate the process with two data sets obtained at 1430, 3500 & 6500 MHz on 2009 March 19, and at 1430 1810 2010 MHz on 2009 April 30.

Example of data reduction for a 7-pointing mosaic on 3c84 at 1430, 3500 & 6500 MHz.

```
#!/bin/csh -vf

echo $0 - Fit JyperK, pointing and Gaussian Primary Beam FWHM to ATA hex7 data

source ~davidm/gemrc.csh

3500:
foreach PNT ( p0 p1 p2 p3 p4 p5 p6 )
  mfcal vis=hexc-3c84-$PNT-3500 line=chan,800,100 select=-auto flux=1
end

gpfit.rb vis="hexc-3c84-p?-3500" options=verbose > gpfit.hexc-3c84-3500
plotpbfits.rb -r 60 -n 4,4 -d /xs gpfit.hexc-3c84-3500
plotpbfits.rb -r 60 -n 4,4 -d gpfit.hexc-3c84-3500.ps/cps gpfit.hexc-3c84-3500

1430:
foreach PNT ( p0 p1 p2 p3 p4 p5 p6 )
  mfcal vis=hexc-3c84-$PNT-1430 line=chan,800,100 select=-auto flux=1
end

gpfit.rb vis="hexc-3c84-p?-1430" options=verbose > gpfit.hexc-3c84-1430
plotpbfits.rb -r 120 -n 4,4 -d /xs gpfit.hexc-3c84-1430
plotpbfits.rb -r 120 -n 4,4 -d gpfit.hexc-3c84-1430.ps/cps gpfit.hexc-3c84-1430

6500:
foreach PNT ( p0 p1 p2 p3 p4 p5 p6 )
  mfcal vis=hexc-3c84-$PNT-6500 line=chan,800,100 select=-auto flux=1
end

gpfit.rb vis="hexc-3c84-p?-6500" options=verbose > gpfit.hexc-3c84-6500
plotpbfits.rb -r 30 -n 4,4 -d /xs gpfit.hexc-3c84-6500
plotpbfits.rb -r 30 -n 4,4 -d gpfit.hexc-3c84-6500.ps/cps gpfit.hexc-3c84
-6500

1430+3500+6500:
plotpbfits.rb -r 120 -n 6,5 -d /xs \
 gpfit.hexc-3c84-1430 \
 gpfit.hexc-3c84-3500 \
```

```
 gpfit.hexc-3c84-6500
plotpbfits.rb -r 120 -n 6,5 -d \
 gpfit.hexc-3c84-1430+3500+6500.ps/cps \
 gpfit.hexc-3c84-1430 \
 gpfit.hexc-3c84-3500 \
 gpfit.hexc-3c84-6500

end:
```

3. RESULTS

3.1. Antenna Gains

The results of the Gaussian fits for the 2009 March 19 data are shown in Tables 1, 2 & 3. Here we used a nominal flux=1 Jy for 3c84, so the peak value (pkval) must be scaled to the flux of 3c84 to obtain the forward gain. The correlator output was un-normalized at this time, so the gain is in units sqrt(Jy/correlation count), i.e. $Gain[Jy/count] = pkval^2 \times (1/Flux3c84)$. The integration times in mfcal must chosen to give the same number of solution intervals for each pointing. Using the default 5 min integration time in mfcal gives 4 gain solutions for these data. The Gaussian fits for these 4 time intervals are shown in Tables 1, 2 & 3.

3.2. Pointing and Squint

The pointing offset is given by az_off el_off in arcmin. In some antennas the X- and Y-polarization have very different pointing offsets, and the antenna suffers from severe pointing squint. This is easily seen in Figure 1 for antennas 23, 24, 28, 32, 42. In some cases the squint (defined at the difference between X- and Y-polarization pointings) is proportional to wavelength, in other cases not. Analysis of more extensive frequency coverage is required to understand how the squint relates to the antenna and feed structure, elevation etc., but the hex-7 mosaic observations and the multifrequency plots clearly provide an excellent tool for obtaining and analysing the necessary data.

3.3. Primary Beam

The primary beamwidth is fitted in azimuth and elevation. The fitted FWHM on the elevation axis appears to be larger than on the azimuth on several antennas, whilst for antennas with large pointing squint the reverse is true, e.g. antenna 23 (See Figures 1 & 2). At 1430 MHz, after omitting antennas with pointing squint greater than 30 arcmin, the mean FWHM is 147.2 +/- 4.2 arcmin in azimuth and 152.3 +/- 4.0 in elevation. At 3500 MHz, after omitting antennas with pointing squint greater than 20 arcmin, the mean FWHM is 59.6 +/- 2.3 arcmin in azimuth and 61.0 +/- 2.1 in elevation. At 6500 MHz, after omitting antennas with pointing squint greater than 10 arcmin, the mean FWHM is 31.4 +/- 1.9 arcmin in azimuth and 32.2 +/- 1.3 in elevation. These measured beamwidths are $\sim$ 5% smaller than the current Gaussian model FWHM 155.2, 63.4 and 34.2 at 1430, 3500 and 6500 MHz respectively. If we get consistent results we should change the nominal FWHM. Since these observations are similar to mosaic projects we should get better mosaic imaging performance using the measured primary beam FWHM. The mean values for both axes are 149.7 +/- 4.0, 59.8 +/- 2.2, and 31.8 +/- 1.6 arcmin at 1430, 3500 and 6500 MHz respectively.

3.4. Bandpass

The Miriad task **mfcal** determines the bandpass for X and Y-polarizations for each antenna. The bandpass is normalized w.r.t. the antenna gain. Figure 3 and 4 show the bandpass amplitude and phase at 1430 MHz. The bandpass at 1430 shows the sinosoidal variation in gain expected for the log periodic feed at 1430 MHz (Welch atal 2009). Figues 5 and 6 show the residual bandpass after calibrating the data using the Miriad task **uvcal** and fitting the corrected data a second time using **mfcal**. The RMS across the channels can be used as an estimate of the antenna-based noise in the data and used to identify antennas with higher noise. The average RMS is 0.025 for X-polarization, and 0.054 for Y-polarization. The expected noise in the bandpass calibration can be estimated using the Miriad task **obsrms**. In the antenna-based calibration, the bandpass for each antenna is determined from the cross with the 25 other antennas currently in the array. **obsrms** estimates the noise from *nants(nants-1)/2* cross correlations, so the effective number of antennas to use in **obsrms** is *nants=5*. Using the nominal *Tsys = 80*, and *jyperk=153*, then *obsrms tsys=80 jyperk=153 nants=5 bw=0.1* gives *rms=0.025* in good agreement with our measurement for the X-polarization, but not for the Y-polarization.

3.5. Bandpass Stability

We can investigate the bandpass stability by transfering the bandpass from the central pointing to the other pointing positions using the Miriad task **gpcopy**, and fitting the corrected data a second time using **mfcal**. Figure 7 and 8 plot the RMS amplitude and phase in the residual bandpass after correcting the data.

```
Table 1. gpfit.hexc-3c84-1430
The full table is at:

http://astro.berkeley.edu/~wright/ata/hex7/gpfit.hexc-3c84-1430


#ant pol fit iters  :  pkval     az_off   el_off  az_fwhm  el_fwhm  |residual|
################################################################################
01 X fit 1 iters 7  : 1.70e+02    2.259  -18.979  147.348  153.964  |X|= 2.1457
01 X fit 2 iters 7  : 1.69e+02    2.427  -17.117  148.932  156.210  |X|= 0.3112
01 X fit 3 iters 7  : 1.72e+02    2.359  -12.736  139.904  151.729  |X|= 2.0964
01 X fit 4 iters 7  : 1.69e+02    1.733  -13.157  146.078  151.289  |X|= 1.4968
01 Y fit 1 iters 7  : 1.55e+02   -3.573  -11.727  153.922  149.529  |X|= 3.0621
01 Y fit 2 iters 7  : 1.56e+02   -2.629   -9.284  149.955  151.525  |X|= 0.8688
01 Y fit 3 iters 7  : 1.56e+02   -1.242   -6.348  143.907  148.004  |X|= 1.4094
01 Y fit 4 iters 7  : 1.53e+02   -3.535   -6.125  151.478  146.462  |X|= 2.2554
```

....

Table 2. gpfit.hexc-3c84-3500
The full table is at:

http://astro.berkeley.edu/˜wright/ata/hex7/gpfit.hexc-3c84-3500

```
#ant pol fit iters  :  pkval     az_off   el_off  az_fwhm  el_fwhm  |residual|
################################################################################
01 X fit 1 iters 7  : 1.25e+02    0.797   -9.143   61.089   63.885  |X|= 2.4941
01 X fit 2 iters 7  : 1.28e+02    2.024   -8.946   59.106   62.547  |X|= 0.6479
01 X fit 3 iters 7  : 1.26e+02    1.864   -6.785   58.831   61.443  |X|= 1.0455
01 X fit 4 iters 7  : 1.28e+02    3.317   -4.983   60.238   63.307  |X|= 1.5310
01 Y fit 1 iters 7  : 1.24e+02    1.660   -6.168   60.849   60.141  |X|= 1.4984
01 Y fit 2 iters 7  : 1.23e+02    2.657   -6.294   60.914   60.118  |X|= 1.0919
01 Y fit 3 iters 7  : 1.22e+02    2.346   -4.522   61.115   60.029  |X|= 0.8483
01 Y fit 4 iters 7  : 1.25e+02    3.839   -2.241   61.277   60.530  |X|= 0.9291
....
```

Table 3. gpfit.hexc-3c84-6500
The full table is at:

http://astro.berkeley.edu/˜wright/ata/hex7/gpfit.hexc-3c84-6500

```
#ant pol fit iters  :  pkval     az_off   el_off  az_fwhm  el_fwhm  |residual|
################################################################################
01 X fit 1 iters 7  : 1.13e+02    1.140   -7.071   31.755   31.949  |X|= 4.0597
01 X fit 2 iters 7  : 1.12e+02    1.919   -6.896   32.318   33.059  |X|= 3.1125
01 X fit 3 iters 7  : 1.12e+02    2.452   -4.719   33.262   33.047  |X|= 2.7846
01 X fit 4 iters 7  : 1.14e+02    2.375   -3.296   32.334   33.395  |X|= 2.6124
01 Y fit 1 iters 7  : 9.13e+01   -1.304   -6.438   31.968   31.794  |X|= 0.7481
01 Y fit 2 iters 7  : 9.06e+01   -0.857   -6.328   32.313   32.583  |X|= 1.8227
01 Y fit 3 iters 8  : 9.15e+01   -0.223   -3.760   33.070   32.477  |X|= 2.5657
01 Y fit 4 iters 7  : 9.22e+01   -0.034   -2.573   32.401   33.399  |X|= 1.1233
....
```

4. DISCUSSION

For multifrequency observations, and comparing survey results, accurate calibration of the flux density scale is needed. For wide field observations, the primary beam illumination must also be calibrated. The case for a homogeneous array of antennas has been well studied. The image fidelity for mosaic observations is limited by pointing and primary beam errors (Cornwell, Holdaway & Uson, 1993; Holdaway, 1998).

The hex-7 mosaic observation and Gaussian fitting provides a fast and accurate method of measuring the antenna gain (corrected for pointing), the antenna pointing, and the primary beam width. The log periodic feed on the ATA antennas provides a frequency dependent gain and illumination of the telescope aperture so it is important to calibrate at the time, focus and frequency of the science observations. If we get consistent results we should change the nominal gain and FWHM to get better image fidelity.

In this memo we present an efficient method for calibrating the antenna gain, pointing, and primary beam widths from observations of compact sources when the primary beam can be characterized by fitting a Gaussian (or other analytic function). These results are relevant to all aperture synthesis arrays, including millimeter/submillimeter wavelength arrays like CARMA and ALMA, and cm/m wavelength arrays like ATA and SKA. The SKA will be a heterogeneous telescope with different primary beam patterns for each antenna station. The primary beam pattern is the product of the voltage patterns for each pair of antenna stations, and is complex valued if the station voltage patterns are not identical. In this case images can be corrected by subtracting from the *uv* data a model of the sky brightness distribution weighted by the complex valued primary beam patterns for each antenna station pair. See, e.g. Wright & Corder (2008).

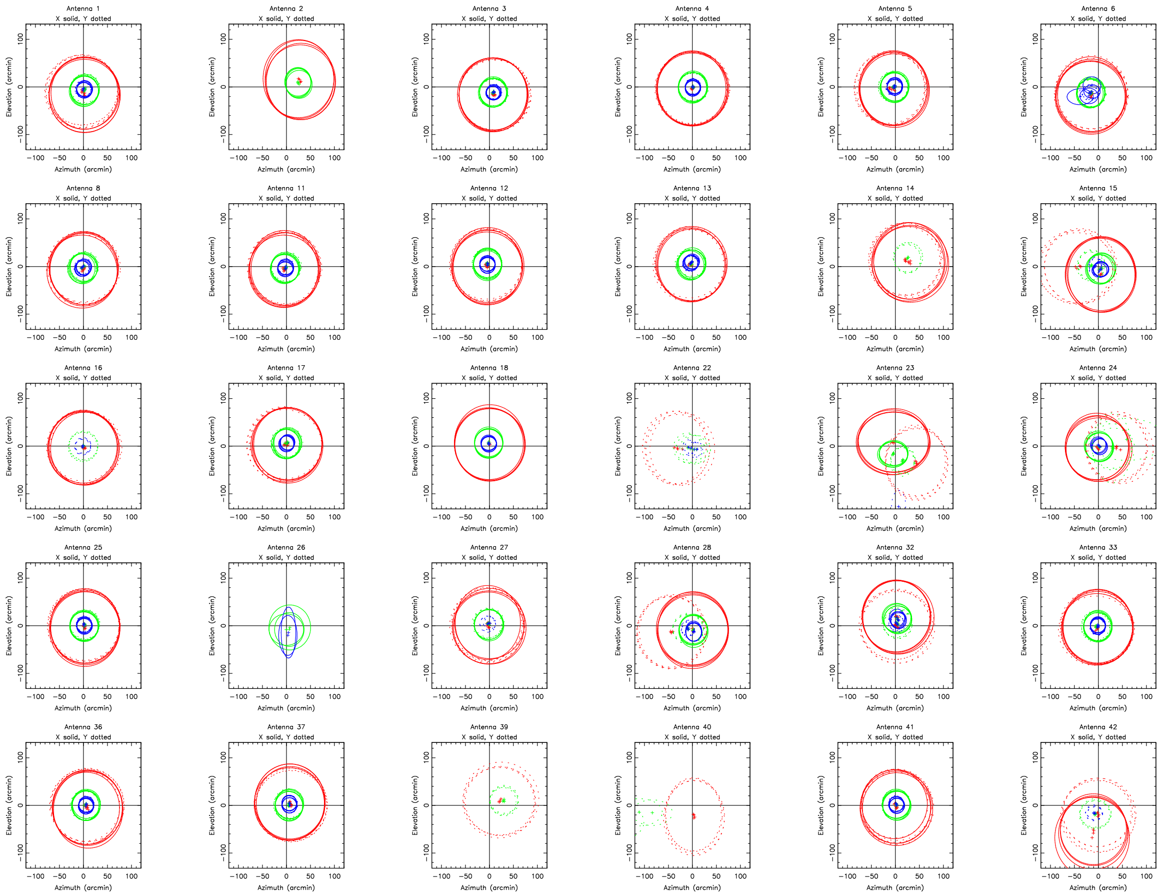

Fig. 1.— Plots the fitted Gaussian pointing offset and primary beam FWHM at 1430 3500 6500 MHz. X-polarization solid, Y-polarization dotted. File: gpfit.hexc-3c84-1430+3500+6500.ps

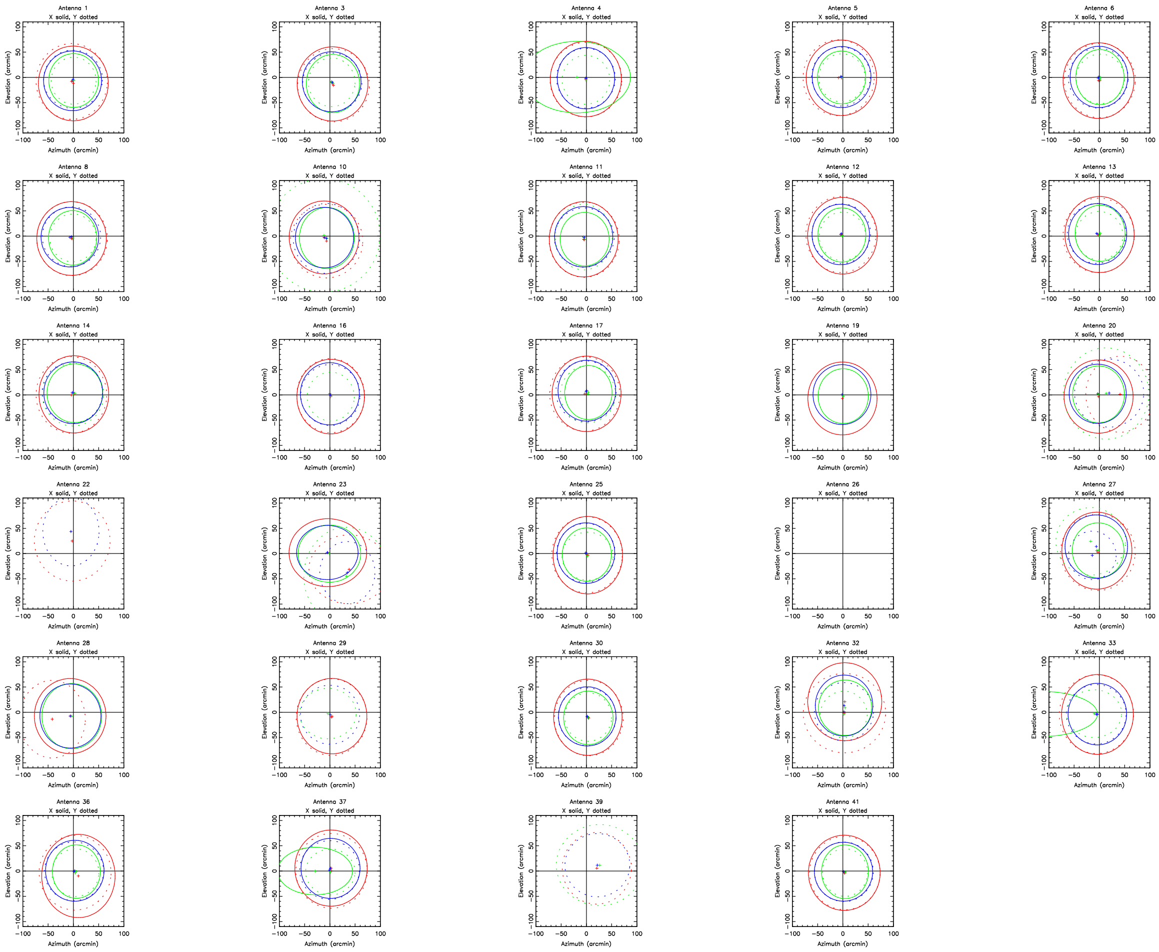

Fig. 2.— Plots the fitted Gaussian pointing offset and primary beam FWHM at 1430 1810 2010 MHz. X-polarization solid, Y-polarization dotted. File: 1430-1810-2010.gpfit.ps

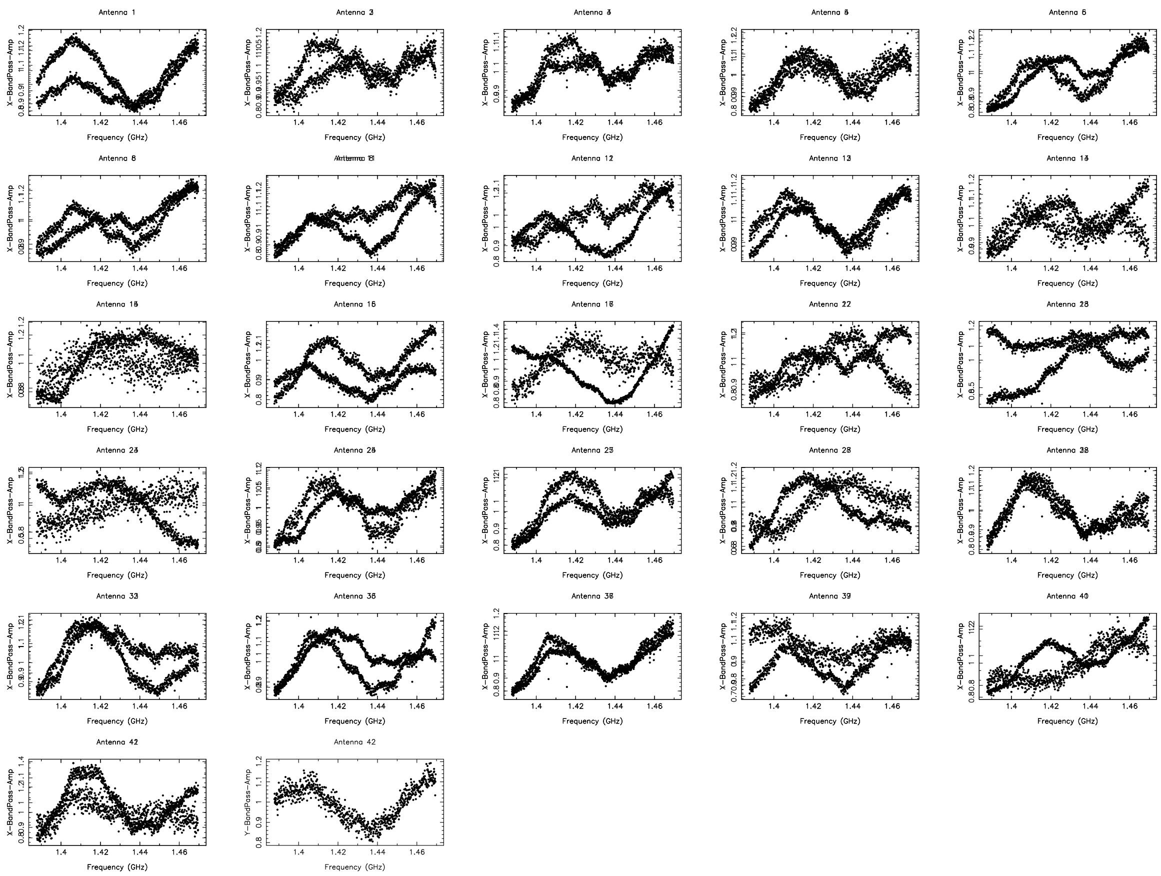

Fig. 3.— Bandpass Amplitude on 3c84 determined by the Miriad task **mfcal** from the central pointing. File: Bandpass-Amp-hexc-3c84-p0-1430.ps

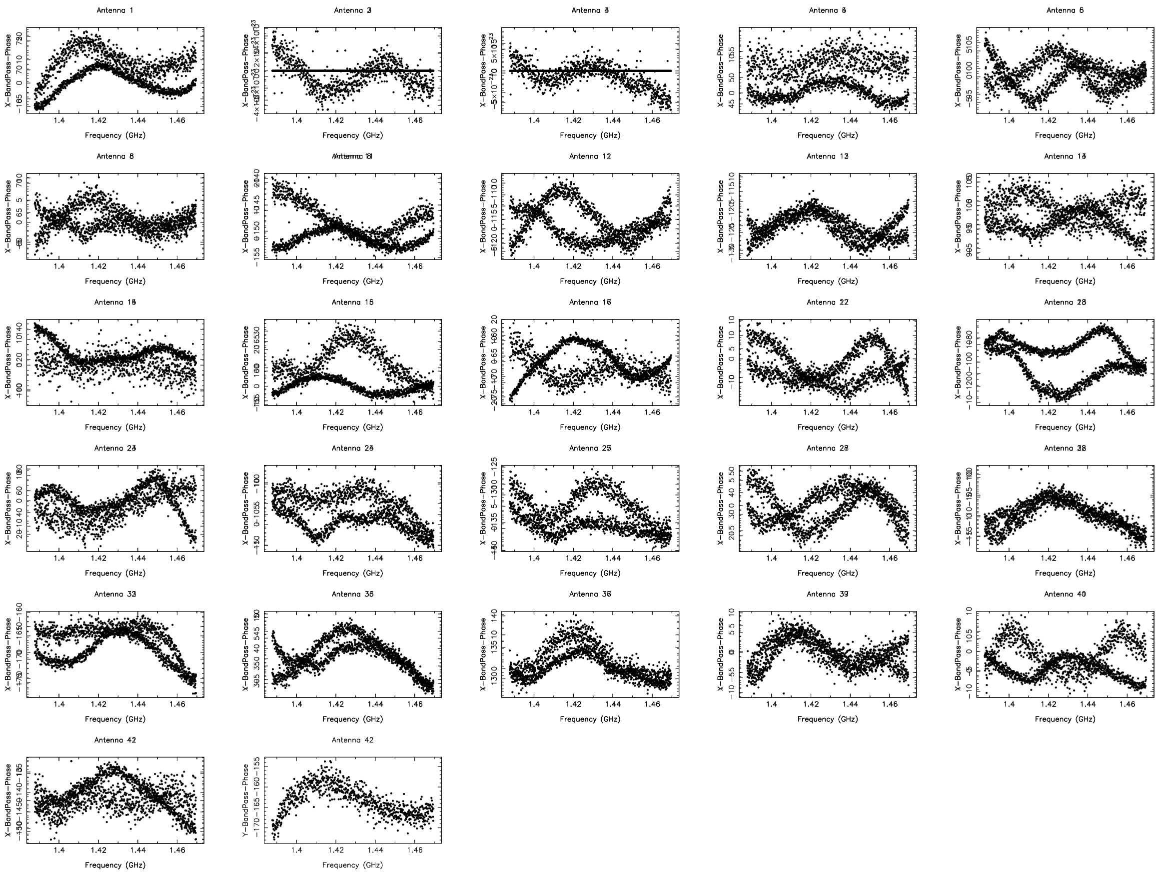

Fig. 4.— Bandpass Phase on 3c84 determined by the Miriad task **mfcal** from the central pointing. File: Bandpass-Phase-hexc-3c84-p0-1430.ps

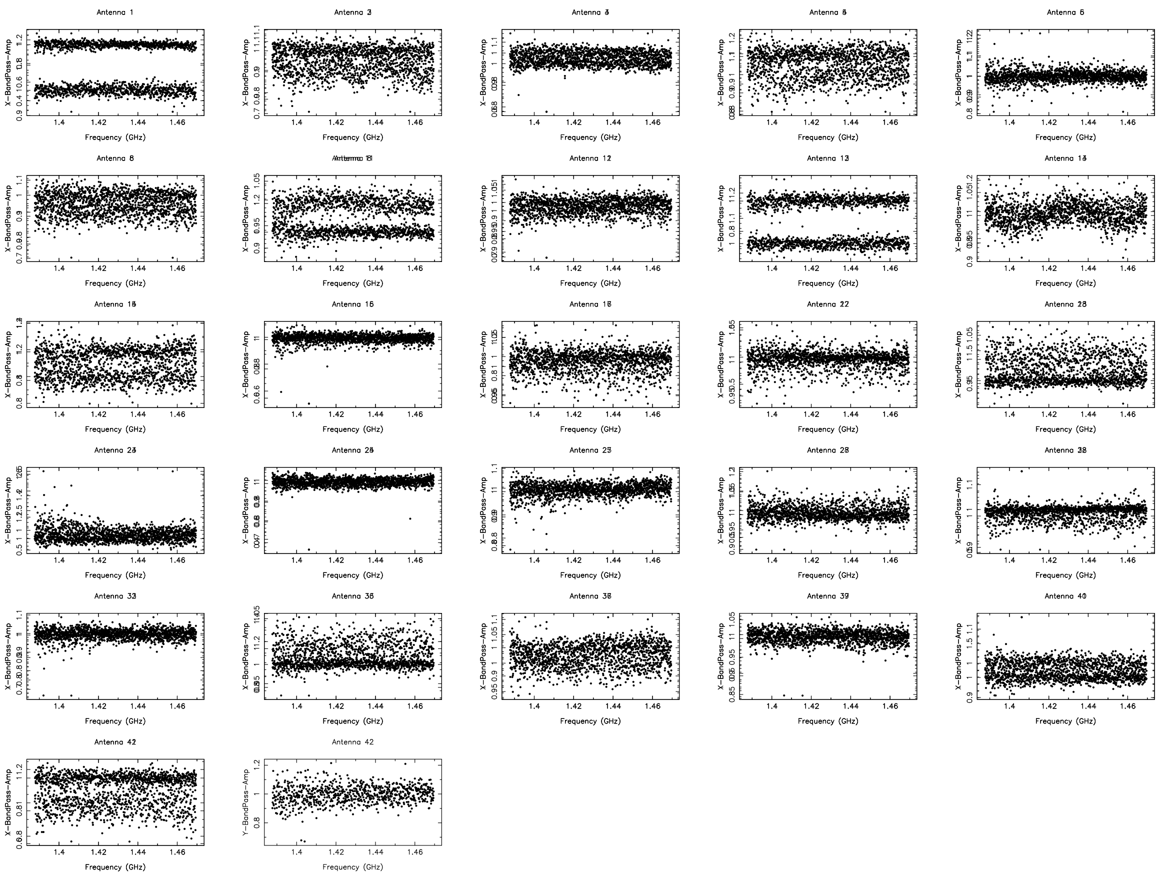

Fig. 5.— Residual Bandpass Amplitude on 3c84 determined by the Miriad task **mfcal** from the central pointing. File: Bandpass-Amp-hexc-3c84-p0-1430.uvcal.ps

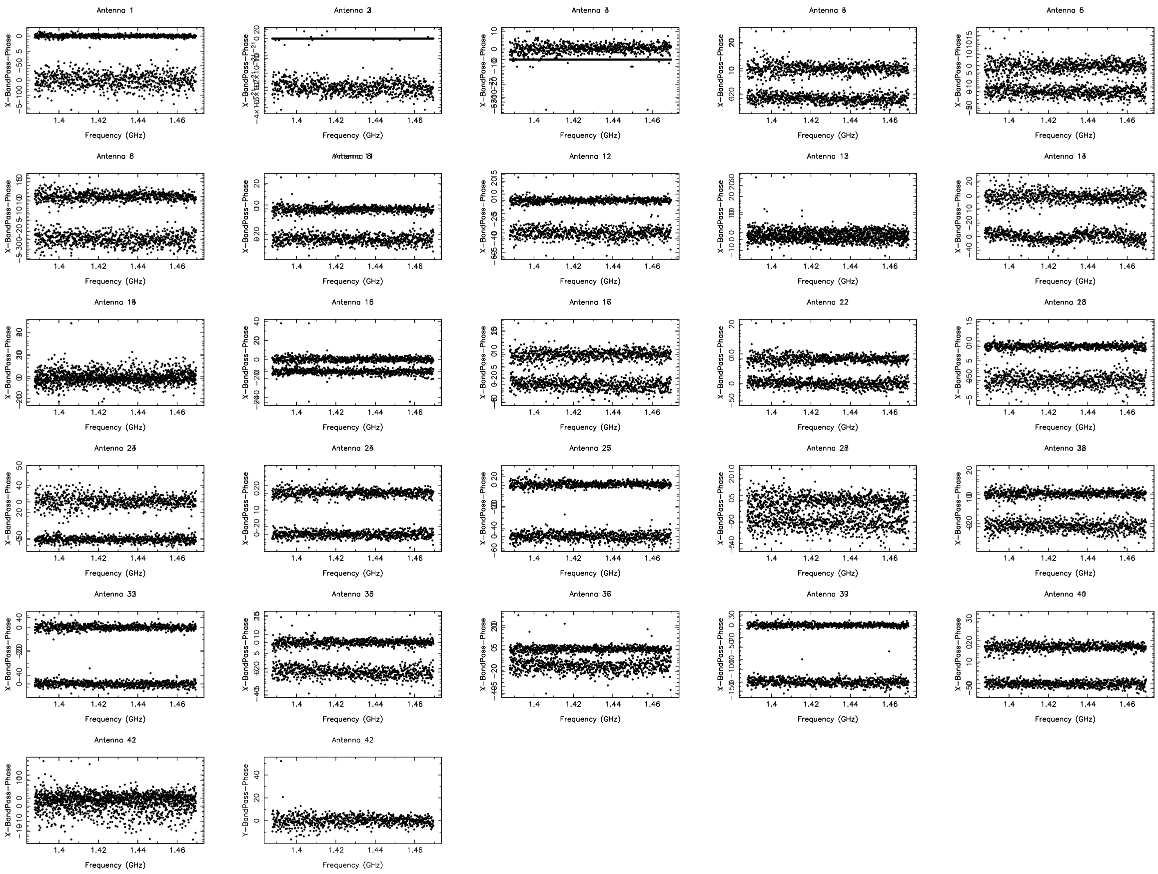

Fig. 6.— Residual Bandpass Phase on 3c84 determined by the Miriad task **mfcal** from the central pointing. File: Bandpass-Phase-hexc-3c84-p0-1430.uvcal.ps

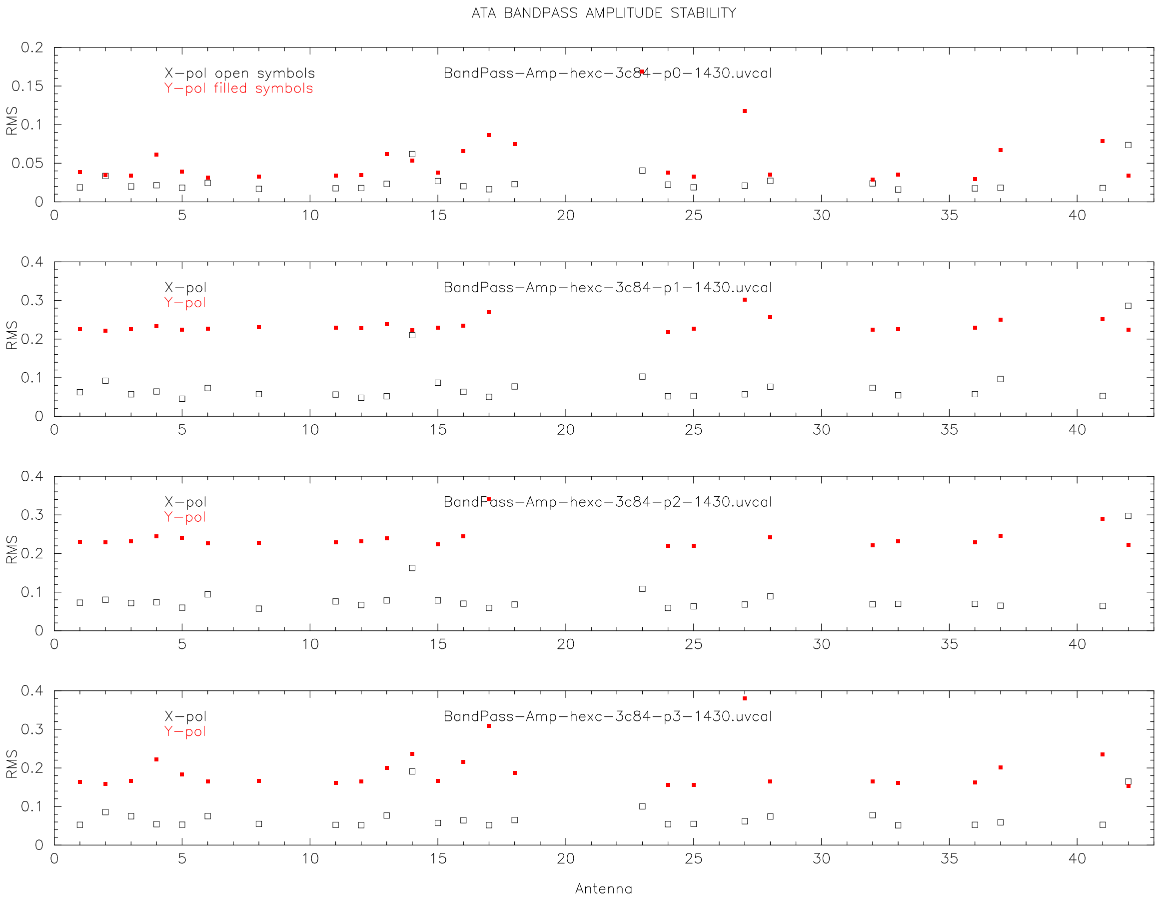

Fig. 7.— Residual Bandpass Amplitude on 3c84 determined by the Miriad task **mfcal** after applying the bandpass from the central pointing. File: Bandpass-Amp-hexc-3c84-p0-1430.uvcal.ps

5. References

Cornwell, T.J., Holdaway, M.A. & Uson, J.M., 1993, A&A 271, 697, *Radio-interferometric imaging of very large objects: implications for array design*

Holdaway, M. A., 1998, *Mosaicing with Interferometer Arrays*, in Synthesis Imaging in Radio Astronomy II, ASP Conference Series, G. B. Taylor, C. L. Carilli and R. A. Perley (eds)

Welch, W.J., etal, 2009, Special Issue of Proceedings of the IEEE: "Advances in Radio Telescopes", Baars,J. Thompson,R., D'Addario, L., eds, 2009, in press. *The Allen Telescope Array: The First Widefield, Panchromatic, Snapshot Radio Camera for Radio Astronomy and SETI.*

Wright, M. & Corder, S., 2008, SKA memo 103, *Deconvolving Primary Beam Patterns from SKA Images*

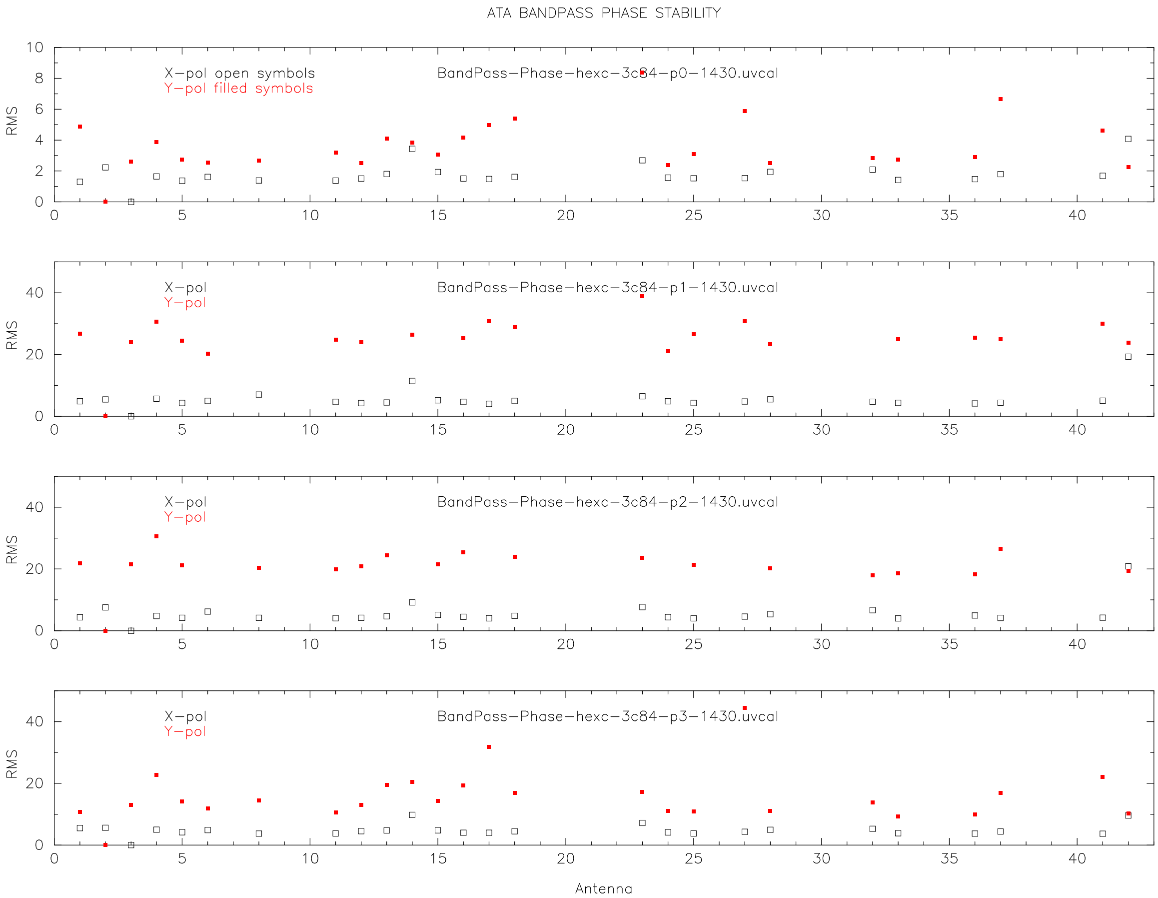

Fig. 8.— Residual Bandpass Phase on 3c84 determined by the Miriad task **mfcal** after applying the bandpass from the central pointing. File: Bandpass-Phase-hexc-3c84-p0-1430.uvcal.ps